

# Diffraction for non-believers

Michele Arneodo<sup>a</sup> and Markus Diehl<sup>b</sup>

<sup>a</sup>Università del Piemonte Orientale, 28100 Novara, Italy

<sup>b</sup>Deutsches Elektronen-Synchrotron DESY, 22603 Hamburg, Germany

## Abstract

Diffraction reactions involving a hard scale can be understood in terms of quarks and gluons. These reactions have become a valuable tool for investigating the low- $x$  structure of the proton and the behavior of QCD in the high-density regime, and they may provide a clean environment to study or even discover the Higgs boson at the LHC. In this paper we give a brief introduction to the description of diffraction in QCD. We focus on key features studied in  $ep$  collisions at HERA and outline challenges for understanding diffractive interactions at the LHC.

## 1 Introduction

In hadron-hadron scattering a substantial fraction of the total cross section is due to diffractive reactions. Figure 1 shows the different types of diffractive processes in the collision of two hadrons: in elastic scattering both projectiles emerge intact in the final state, whereas single or double diffractive dissociation corresponds to one or both of them being scattered into a low-mass state; the latter has the same quantum numbers as the initial hadron and may be a resonance or continuum state. In all cases, the energy of the outgoing hadrons  $a, b$  or the states  $X, Y$  is approximately equal to that of the incoming beam particles, to within a few per cent. The two (groups of) final-state particles are well separated in phase space and in particular have a large gap in rapidity between them.

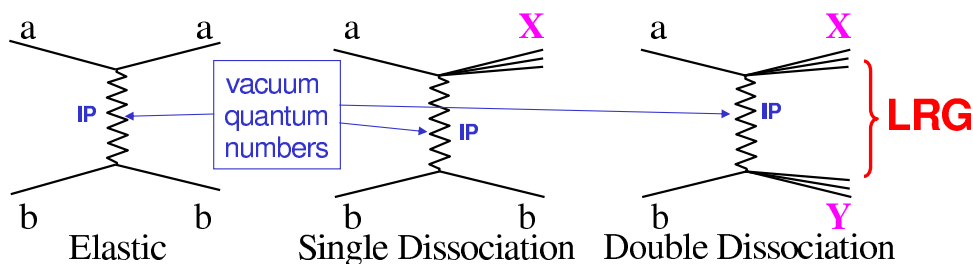


**Fig. 1:** Elastic scattering, single diffractive dissociation and double diffractive dissociation in the collision of two hadrons  $a$  and  $b$ . The two (groups of) final-state hadrons are separated by a large rapidity gap (LRG). The zigzag lines denote the exchange of a Pomeron ( $IP$ ) in the  $t$ -channel. There are further graphs, not shown, with multiple Pomeron exchange.

Diffractive hadron-hadron scattering can be described within Regge theory (see e.g. [1]). In this framework, the exchange of particles in the  $t$ -channel is summed coherently to give the exchange of so-called “Regge trajectories”. Diffraction is characterized by the exchange of a specific trajectory, the “Pomeron”, which has the quantum numbers of the vacuum. Regge theory has spawned a successful phenomenology of soft hadron-hadron scattering at high energies. Developed in the 1960s, it predates the theory of the strong interactions, QCD, and is based on general concepts such as dispersion relations. Subsequently it was found that QCD perturbation theory in the high-energy limit can be organized following the general concepts of Regge theory; this framework is often referred to as BFKL after the authors of the seminal papers [2].

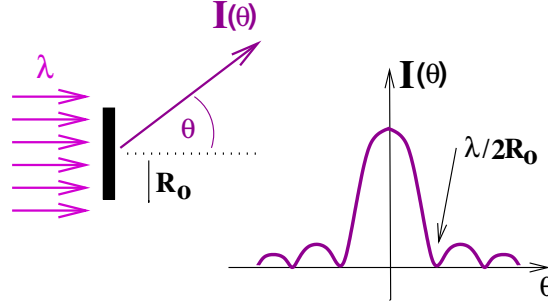


**Fig. 2:** Distribution of the intensity  $I$  in the diffraction of light of wavelength  $\lambda$  from a circular target of size  $R_0$ .

It is clear that a  $t$ -channel exchange leading to a large rapidity gap in the final state must carry zero net color: if color were exchanged, the color field would lead to the production of further particles filling any would-be rapidity gap. In QCD, Pomeron exchange is described by the exchange of two interacting gluons with the vacuum quantum numbers.

The effort to understand diffraction in QCD has received a great boost from studies of diffractive events in  $ep$  collisions at HERA (see e.g. [3] for further reading and references). The essential results of these studies are discussed in the present paper and can be summarized as follows:

- Many aspects of diffraction are well understood in QCD when a hard scale is present, which allows one to use perturbative techniques and thus to formulate the dynamics in terms of quarks and gluons. By studying what happens when the hard scale is reduced towards the non-perturbative region, it may also be possible to shed light on soft diffractive processes.
- Diffraction has become a tool to investigate low-momentum partons in the proton, notably through the study of diffractive parton densities in inclusive processes and of generalized parton distributions in exclusive ones. Diffractive parton densities can be interpreted as conditional probabilities to find a parton in the proton when the final state of the process contains a fast proton of given four-momentum. Generalized parton distributions, through their dependence on both longitudinal and transverse variables, provide a three-dimensional picture of the proton in high-energy reactions.
- A fascinating link has emerged between diffraction and the physics of heavy-ion collisions through the concept of saturation, which offers a new window on QCD dynamics in the regime of high parton densities.

Perhaps unexpectedly, the production of the Higgs boson in diffractive  $pp$  collisions is drawing more and more attention as a clean channel to study the properties of a light Higgs boson or even discover it. This is an example of a new theoretical challenge: to adapt and apply the techniques for the QCD description of diffraction in  $ep$  collisions to the more complex case of  $pp$  scattering at the LHC. A first glimpse of phenomena to be expected there is provided by the studies of hard diffraction in  $p\bar{p}$  collisions at the Tevatron.

### 1.1 A digression on the nomenclature: why “diffraction” ?

Physics students first encounter the term “diffraction” in optics. Light of wavelength  $\lambda$  impinging on a black disk of radius  $R_0$  produces on a distant screen a diffraction pattern, characterized by a large forward peak for scattering angle  $\theta = 0$  (the “diffraction peak”) and a series of symmetric minima and maxima, with the first minimum at  $\theta_{\min} \simeq \pm\lambda/(2R_0)$  (Fig. 2). The intensity  $I$  as a function of the scattering angle  $\theta$  is given by

$$\frac{I(\theta)}{I(\theta = 0)} = \frac{[2J_1(x)]^2}{x^2} \simeq 1 - \frac{R_0^2}{4}(k\theta)^2, \quad (1)$$

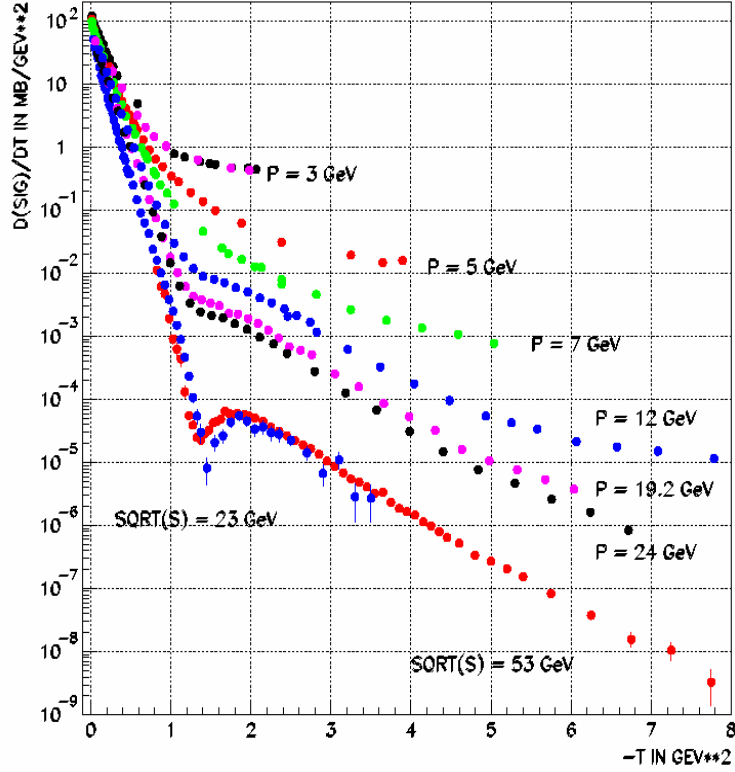


**Fig. 3:** Compilation of proton-proton elastic cross section data as a function of  $t$ . The symbol  $P$  indicates the momentum of the incoming proton in a fixed target experiment and  $\sqrt{s}$  the center-of-mass energy in a  $pp$  collider setup.

where  $J_1$  is the Bessel function of the first order and  $x = kR_0 \sin \theta \simeq kR_0 \theta$  with  $k = 2\pi/\lambda$ . The diffraction pattern is thus related to the size of the target and to the wavelength of the light beam.

As shown in Fig. 3, the differential cross section  $d\sigma/dt$  for elastic proton-proton scattering,  $pp \rightarrow pp$ , bears a remarkable resemblance to the diffraction pattern just described (see e.g. [4]). At low values of  $|t|$  one has

$$\frac{\frac{d\sigma}{dt}(t)}{\frac{d\sigma}{dt}(t=0)} \simeq e^{-b|t|} \simeq 1 - b(P\theta)^2, \quad (2)$$

where  $|t| \simeq (P\theta)^2$  is the absolute value of the squared four-momentum transfer,  $P$  is the incident proton momentum and  $\theta$  is the scattering angle. The  $t$ -slope  $b$  can be written as  $b = R^2/4$ , where once again  $R$  is related to the target size (or more precisely to the transverse distance between projectile and target). A dip followed by a secondary maximum has also been observed, with the value of  $|t|$  at which the dip appears decreasing with increasing proton momentum. It is hence not surprising that the term diffraction is used for elastic  $pp$  scattering. Similar  $t$  distributions have been observed for the other diffractive reactions mentioned above, leading to the use of the term diffraction for all such processes.

## 1.2 Diffraction at HERA ?!

Significant progress in understanding diffraction has been made at the  $ep$  collider HERA, where 27.5 GeV electrons or positrons collide with 820 or 920 GeV protons. This may sound peculiar: diffraction is a typical hadronic process while  $ep$  scattering at HERA is an electro-weak reaction, where the electron

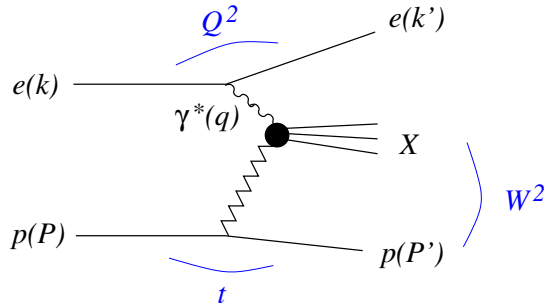


**Fig. 4:** Schematic diagram of inclusive diffractive DIS,  $ep \rightarrow eXp$ . Four-momenta are indicated in parentheses.

radiates a virtual photon (or a  $Z$  or  $W$  boson), which then interacts with the proton.<sup>1</sup> To understand this, it is useful to look at  $ep$  scattering in a frame where the virtual photon moves very fast (for instance in the proton rest frame, where the  $\gamma^*$  has a momentum of up to about 50 TeV at HERA). The virtual photon can fluctuate into a quark-antiquark pair. Because of its large Lorentz boost, this virtual pair has a lifetime much longer than a typical strong interaction time. In other words, the photon fluctuates into a pair long before the collision, and it is the pair that interacts with the proton. This pair is a small color dipole. Since the interaction between the pair and the proton is mediated by the strong interaction, diffractive events are possible.

An advantage of studying diffraction in  $ep$  collisions is that, for sufficiently large photon virtuality  $Q^2$ , the typical transverse dimensions of the dipole are small compared to the size of a hadron. Then the interaction between the quark and the antiquark, as well as the interaction of the pair with the proton, can be treated perturbatively. With decreasing  $Q^2$  the color dipole becomes larger, and at very low  $Q^2$  these interactions become so strong that a description in terms of quarks and gluons is no longer justified. We may then regard the photon as fluctuating into a vector meson – this is the basis of the well-known vector meson dominance model – and can therefore expect to see diffractive reactions very similar to those in hadron-hadron scattering.

A different physical picture is obtained in a frame where the incident proton is very fast. Here, the diffractive reaction can be seen as the deep inelastic scattering (DIS) of a virtual photon on the proton target, with a very fast proton in the final state. One can thus expect to probe partons in the proton in a very specific way. For suitable diffractive processes there are in fact different types of QCD factorization theorems, which bear out this expectation (see Sects. 2 and 3).

## 2 Inclusive diffractive scattering in $ep$ collisions

Figure 4 shows a schematic diagram of inclusive diffractive DIS. The following features are important:

- The proton emerges from the interaction carrying a large fraction  $x_L$  of the incoming proton momentum. Diffractive events thus appear as a peak at  $x_L \approx 1$ , the diffractive peak, which at HERA approximately covers the region  $0.98 < x_L < 1$  (see the left panel of Fig. 5). The right panel of Fig. 5 shows that large values of  $|t|$  are exponentially suppressed, similarly to the case of elastic  $pp$  scattering we discussed in Sect. 1.1. These protons remain in the beam-pipe and can only be measured with detectors located inside the beam-pipe.
- The collision of the virtual photon with the proton produces a hadronic final state  $X$  with the photon quantum numbers and invariant mass  $M_X$ . A large gap in rapidity (or pseudorapidity) is present between  $X$  and the final-state proton. Figure 6 shows a typical diffractive event at HERA.

<sup>1</sup>For simplicity we will speak of a virtual photon in the following, keeping in mind that one can have a weak gauge boson instead.

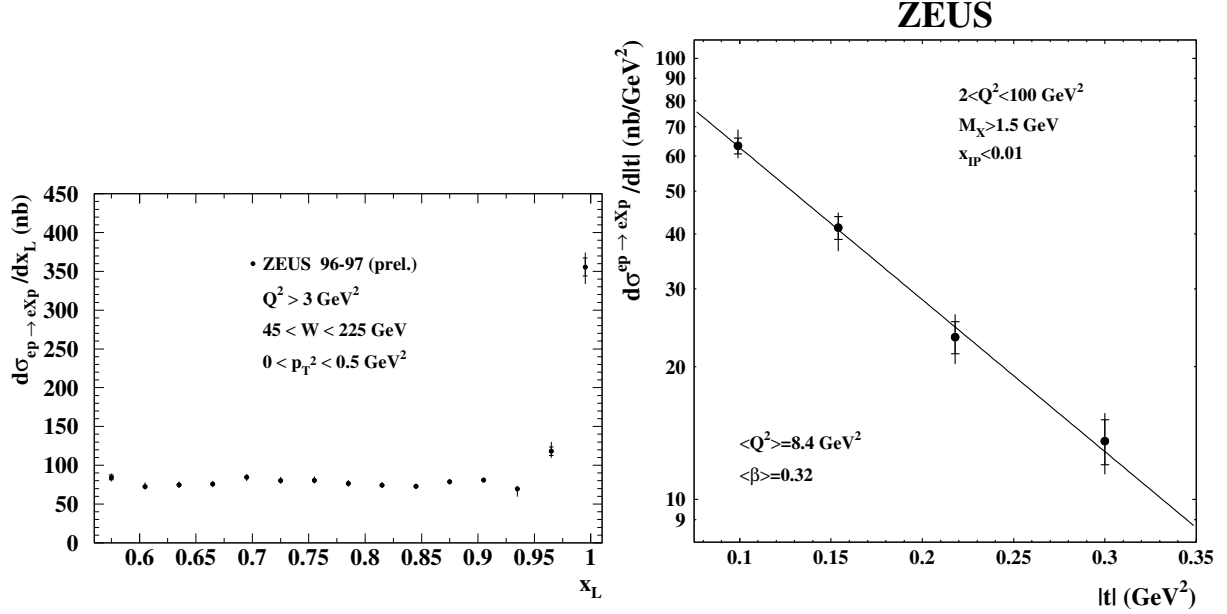


**Fig. 5:** Left: Differential cross section  $d\sigma/dx_L$  for the process  $ep \rightarrow eXp$  (from [5]). The diffractive peak at  $x_L \approx 1$  is clearly visible. Right: Differential cross section  $d\sigma/dt$  for the same process for  $x_L > 0.99$  (from [6]). The average  $|t|$  of this spectrum is  $\langle |t| \rangle \approx 0.15 \text{ GeV}^2$ .

Diffractive  $ep$  scattering thus combines features of hard and soft scattering. The electron receives a large momentum transfer; in fact  $Q^2$  can be in the hundreds of  $\text{GeV}^2$ . In contrast, the proton emerges with its momentum barely changed.

## 2.1 Diffractive structure functions

The kinematics of  $\gamma^*p \rightarrow Xp$  can be described by the invariants  $Q^2 = -q^2$  and  $t = (P - P')^2$ , and by the scaling variables  $x_P$  and  $\beta$  given by

$$x_P = \frac{(P - P') \cdot q}{P \cdot q} = \frac{Q^2 + M_X^2 - t}{W^2 + Q^2 - M_p^2}, \quad \beta = \frac{Q^2}{2(P - P') \cdot q} = \frac{Q^2}{Q^2 + M_X^2 - t}, \quad (3)$$

where  $W^2 = (P + q)^2$  and the four-momenta are defined in Fig. 4. The variable  $x_P$  is the fractional momentum loss of the incident proton, related as  $x_P \simeq 1 - x_L$  to the variable  $x_L$  introduced above. The quantity  $\beta$  has the form of a Bjorken variable defined with respect to the momentum  $P - P'$  lost by the initial proton instead of the initial proton momentum  $P$ . The usual Bjorken variable  $x_B = Q^2/(2P \cdot q)$  is related to  $\beta$  and  $x_P$  as  $\beta x_P = x_B$ .

The cross section for  $ep \rightarrow eXp$  in the one-photon exchange approximation can be written in terms of diffractive structure functions  $F_2^{D(4)}$  and  $F_L^{D(4)}$  as

$$\frac{d\sigma^{ep \rightarrow eXp}}{d\beta dQ^2 dx_P dt} = \frac{4\pi\alpha_{\text{em}}^2}{\beta Q^4} \left[ \left(1 - y + \frac{y^2}{2}\right) F_2^{D(4)}(\beta, Q^2, x_P, t) - \frac{y^2}{2} F_L^{D(4)}(\beta, Q^2, x_P, t) \right], \quad (4)$$

in analogy with the way  $d\sigma^{ep \rightarrow eX}/(dx_B dQ^2)$  is related to the structure functions  $F_2$  and  $F_L$  for inclusive DIS,  $ep \rightarrow eX$ . Here  $y = (P \cdot q)/(P \cdot k)$  is the fraction of energy lost by the incident lepton in the proton rest frame. The structure function  $F_L^{D(4)}$  corresponds to longitudinal polarization of the virtual photon;

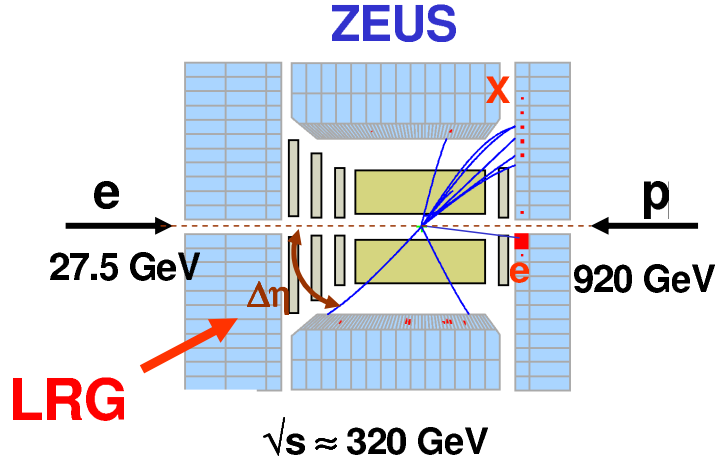


**Fig. 6:** A DIS event with a large rapidity gap (LRG) observed with the ZEUS detector at HERA. The scattered proton escapes into the beam-pipe. The symbol  $\Delta\eta$  denotes the difference in pseudorapidity between the scattered proton and the most forward particle of the observed hadronic system  $X$ . Pseudorapidity is defined as  $\eta = -\ln \tan(\theta/2)$  in terms of the polar angle  $\theta$  measured with respect to the incoming proton direction, which is defined as “forward”.

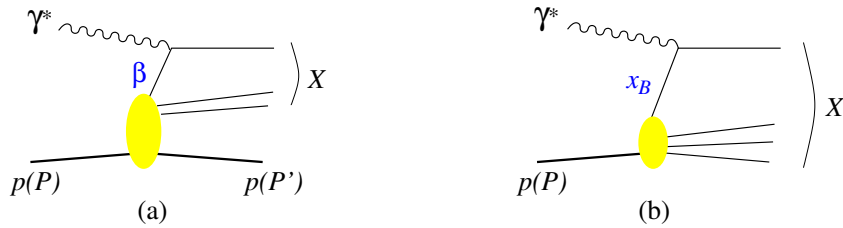


**Fig. 7:** Parton model diagrams for deep inelastic diffractive (a) and inclusive (b) scattering. The variable  $\beta$  is the momentum fraction of the struck quark with respect to  $P - P'$ , and  $x_B$  its momentum fraction with respect to  $P$ .

its contribution to the cross section is small in a wide range of the experimentally accessible kinematic region (in particular at low  $y$ ). The structure function  $F_2^{D(3)}$  is obtained from  $F_2^{D(4)}$  by integrating over  $t$ :

$$F_2^{D(3)}(\beta, Q^2, x_P) = \int dt F_2^{D(4)}(\beta, Q^2, x_P, t). \quad (5)$$

In a parton model picture, inclusive diffraction  $\gamma^* p \rightarrow Xp$  proceeds by the virtual photon scattering on a quark, in analogy to inclusive scattering (see Fig. 7). In this picture,  $\beta$  is the momentum fraction of the struck quark with respect to the exchanged momentum  $P - P'$  (indeed the allowed kinematical range of  $\beta$  is between 0 and 1). The diffractive structure function describes the proton structure in these specific processes with a fast proton in the final state.  $F_2^D$  may also be viewed as describing the structure of whatever is exchanged in the  $t$ -channel in diffraction, i.e. of the Pomeron (if multiple Pomeron exchange can be neglected). It is however important to bear in mind that the Pomeron in QCD cannot be interpreted as a particle on which the virtual photon scatters, as we will see in Sect. 2.5.

Figures 8 and 9 show recent H1 data [7] on  $F_2^{D(3)}$  at fixed  $x_P$  as a function of  $\beta$  for different  $Q^2$  bins, and as a function of  $Q^2$  for different bins of  $\beta$ .<sup>2</sup> The data have two remarkable features:

<sup>2</sup>To be precise, the H1 data are for the so-called reduced diffractive cross section, which equals  $F_2^{D(3)}$  if  $F_L^D$  can be neglected.

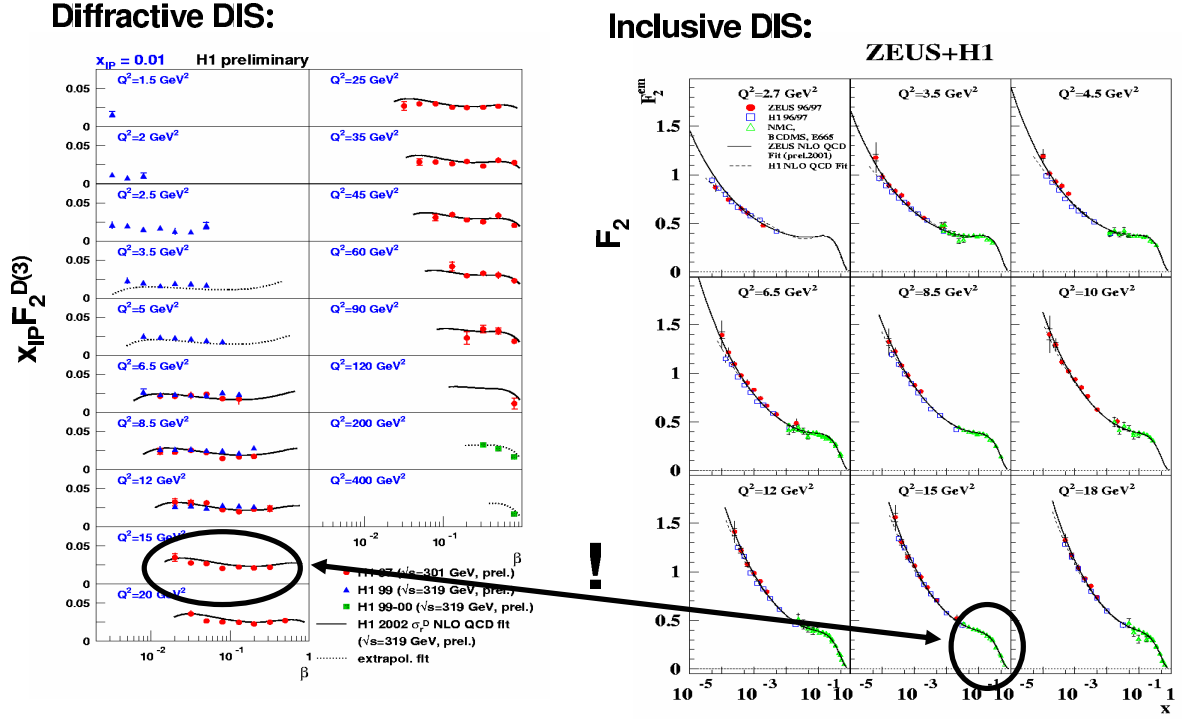


**Fig. 8:** Left: the diffractive structure function of the proton as a function of  $\beta$  (from [7]). Right: the structure function of the proton as a function of  $x_B$  (from [8]). The two highlighted bins show the different shapes of  $F_2^D$  and  $F_2$  in corresponding ranges of  $\beta$  and  $x_B$  at equal  $Q^2$ .

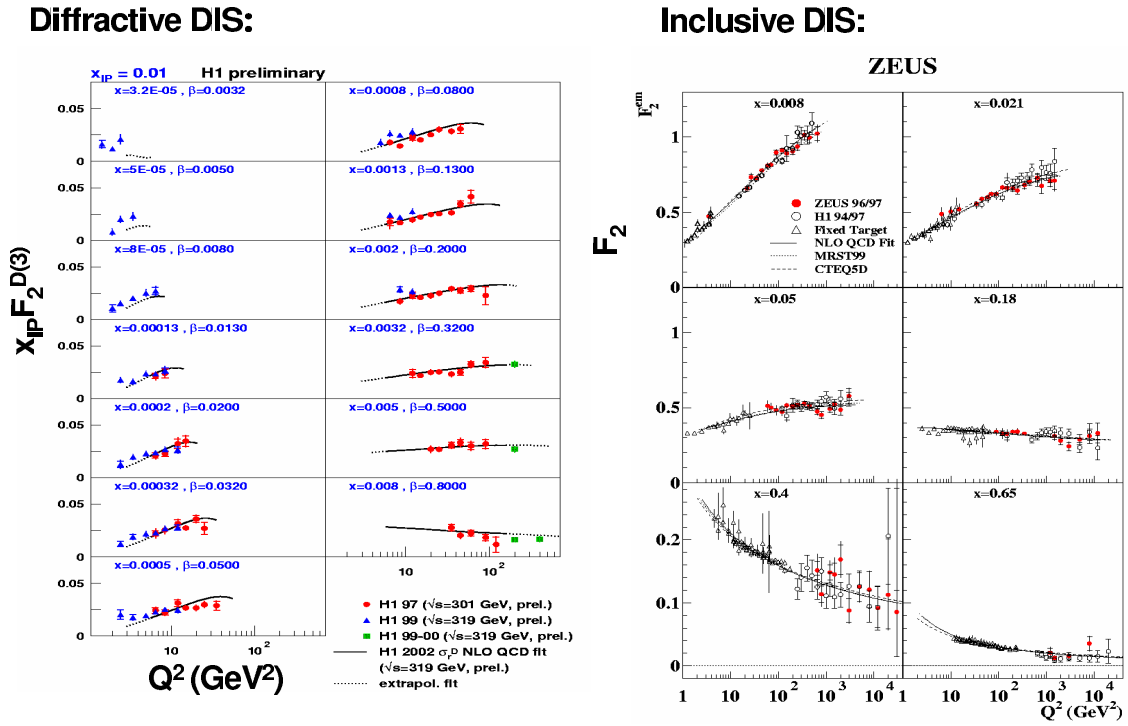


**Fig. 9:** Left: the diffractive structure function of the proton as a function of  $Q^2$  (from [7]). Right: the structure function of the proton as a function of  $Q^2$  (from [9]).

- $F_2^D$  is largely flat in the measured  $\beta$  range. Keeping in mind the analogy between  $\beta$  in diffractive DIS and  $x_B$  in inclusive DIS, this is very different from the behavior of the “usual” structure function  $F_2$ , which strongly decreases for  $x_B \gtrsim 0.2$  (see Fig. 8).
- The dependence on  $Q^2$  is logarithmic, i.e. one observes approximate Bjorken scaling. This indicates the applicability of the parton model picture to inclusive  $\gamma^*p$  diffraction. The structure function  $F_2^D$  increases with  $Q^2$  for all  $\beta$  values except the highest. This is reminiscent of the scaling violations of  $F_2$ , except that  $F_2$  rises with  $Q^2$  only for  $x_B \lesssim 0.2$  and that the scaling violations become negative at higher  $x_B$  (see Fig. 9). In the proton, negative scaling violations reflect the presence of the valence quarks radiating gluons, while positive scaling violations are due to the increase of the sea quark and gluon densities as the proton is probed with higher resolution. The  $F_2^D$  data thus suggest that the partons resolved in diffractive events are predominantly gluons. This is not too surprising if one bears in mind that these partons carry only a small part of the proton momentum: the struck quark in the diagram of Fig. 7a has a momentum fraction  $\beta x_{\mathbb{P}} = x_B$  with respect to the incident proton, and  $x_{\mathbb{P}} \lesssim 0.02 - 0.03$  in diffractive events.

## 2.2 Diffractive parton distributions

The conclusion just reached can be made quantitative by using the QCD factorization theorem for inclusive diffraction,  $\gamma^*p \rightarrow Xp$ , which formalizes the parton model picture we have already invoked in our discussion. According to this theorem, the diffractive structure function, in the limit of large  $Q^2$  at fixed  $\beta$ ,  $x_{\mathbb{P}}$  and  $t$ , can be written as [10–12]

$$F_2^{D(4)}(\beta, Q^2, x_{\mathbb{P}}, t) = \sum_i \int_{\beta}^1 \frac{dz}{z} C_i\left(\frac{\beta}{z}\right) f_i^D(z, x_{\mathbb{P}}, t; Q^2), \quad (6)$$

where the sum is over partons of type  $i$ . The coefficient functions  $C_i$  describe the scattering of the virtual photon on the parton and are exactly the same as in inclusive DIS. In analogy to the usual parton distribution functions (PDFs), the diffractive PDFs  $f_i^D(z, x_{\mathbb{P}}, t; Q^2)$  can be defined as operator matrix elements in a proton state, and their dependence on the scale  $Q^2$  is given by the DGLAP evolution equations. In parton model language, they can be interpreted as conditional probabilities to find a parton  $i$  with fractional momentum  $zx_{\mathbb{P}}$  in a proton, probed with resolution  $Q^2$  in a process with a fast proton in the final state (whose momentum is specified by  $x_{\mathbb{P}}$  and  $t$ ).

During the workshop, several fits of the available  $F_2^D$  data were discussed which are based on the factorization formula (6) at next-to-leading order (NLO) in  $\alpha_s$  [13,14]. Figure 10 compares the diffractive PDFs from an earlier H1 fit [7] to those from the fit of the ZEUS data [15] by Schilling and Newman [13]. As expected the density of gluons is larger than that of quarks, by about a factor 5–10. Discrepancies between the two sets are evident, and it remains to be clarified to which extent they reflect differences in the fitted data. Martin, Ryskin and Watt [16] have argued that the leading-twist formula (6) is inadequate in large parts of the measured kinematics, and performed a fit to a modified expression which includes an estimate of power-suppressed effects. The discrepancies between the various diffractive PDFs, while not fully understood, may be taken as an estimate of the uncertainties on these functions at this point in time. A precise and consistent determination of the diffractive PDFs and their uncertainties is one of the main tasks the HERA community has to face in the near future. They are a crucial input for predicting cross sections of inclusive diffractive processes at the LHC.

## 2.3 Diffractive hard-scattering factorization

Like usual parton densities, diffractive PDFs are process-independent functions. They appear not only in inclusive diffraction but also in other processes where diffractive hard-scattering factorization holds. In analogy with Eq. (6), the cross section of such a process can be evaluated as the convolution of the relevant parton-level cross section with the diffractive PDFs. For instance, the cross section for charm

### NLO QCD fits to H1 and ZEUS data

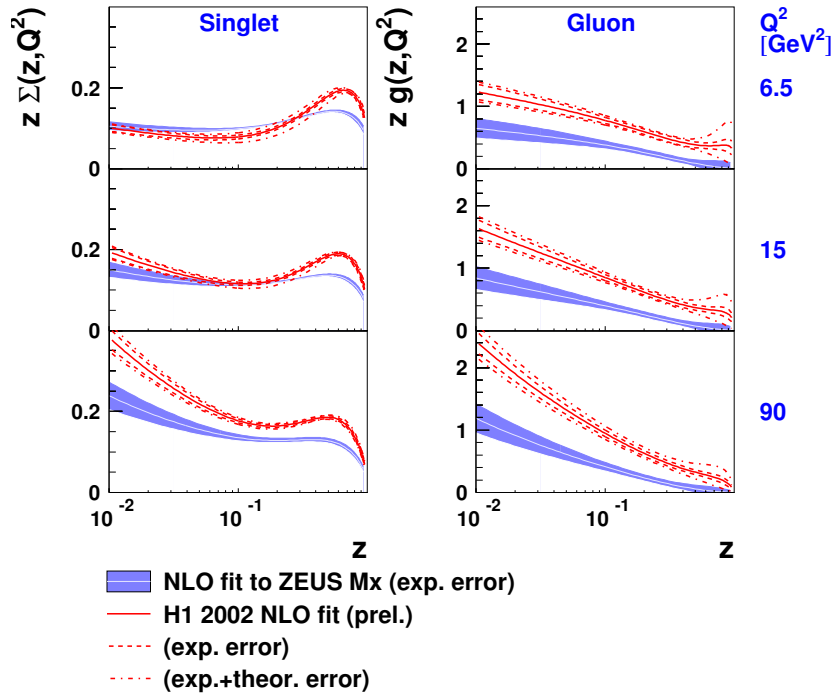


**Fig. 10:** Diffractive quark singlet and gluon distributions obtained from fits to H1 [7] and ZEUS [15] data (from [13]).

### H1 Diffractive DIS Dijets

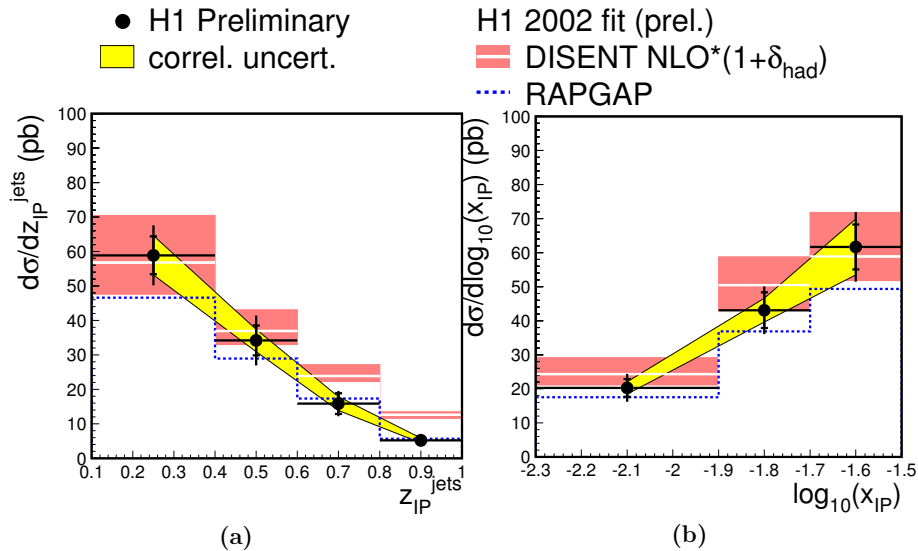


**Fig. 11:** Cross section for dijet production in diffractive DIS, compared with the expectations based on the diffractive PDFs [7] (from [17]). The variable  $z_{IP}^{\text{jets}}$  estimates the fractional momentum of the parton entering the hard subprocess.

production in diffractive DIS can be calculated at leading order in  $\alpha_s$  from the  $\gamma^*g \rightarrow c\bar{c}$  cross section and the diffractive gluon distribution. An analogous statement holds for jet production in diffractive DIS. Both processes have been analyzed at next-to-leading order in  $\alpha_s$ .

As an example, Fig. 11 shows a comparison between the measured cross sections for diffractive dijet production and the expectations based on diffractive PDFs extracted from a fit to  $F_2^D$ . These data lend support to the validity of hard-scattering factorization in diffractive  $\gamma^*p$  interactions. For further discussion we refer the reader to [18].

## 2.4 Limits of diffractive hard-scattering factorization: hadron-hadron collisions

A natural question to ask is whether one can use the diffractive PDFs extracted at HERA to describe hard diffractive processes such as the production of jets, heavy quarks or weak gauge bosons in  $p\bar{p}$  collisions at the Tevatron. Figure 12 shows results on diffractive dijet production from the CDF collaboration [19] compared to the expectations based on the diffractive PDFs [6, 7] from HERA. The discrepancy is spectacular: the fraction of diffractive dijet events at CDF is a factor 3 to 10 smaller than would be expected on the basis of the HERA data. The same type of discrepancy is consistently observed in all hard diffractive processes in  $p\bar{p}$  events, see e.g. [20]. In general, while at HERA hard diffraction contributes a fraction of order 10% to the total cross section, it contributes only about 1% at the Tevatron.

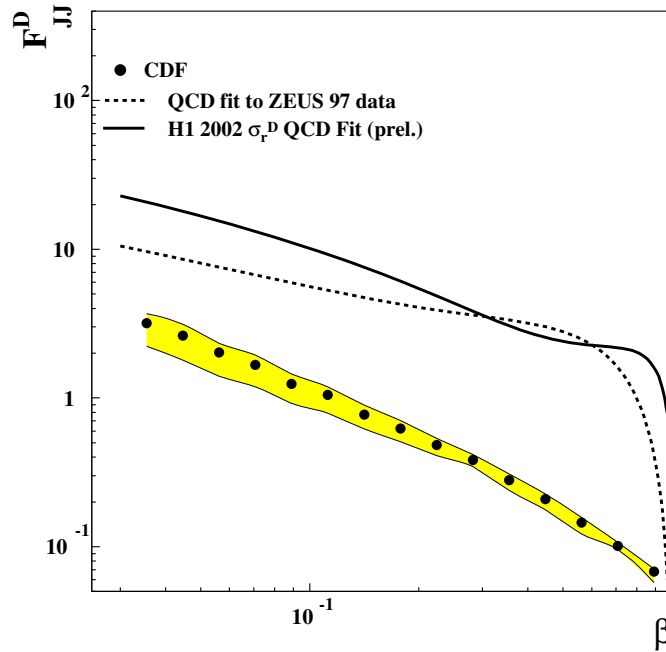


**Fig. 12:** CDF results for the cross section of diffractive dijet production with a leading antiproton in  $p\bar{p}$  collisions (expressed in terms of a structure function  $F_{JJ}^D$ ), compared with the predictions obtained from the diffractive PDFs [6] and [7] extracted at HERA (from [21]). See also the analogous plot in the original CDF publication [19].

In fact, diffractive hard-scattering factorization does not apply to hadron-hadron collisions [11,12]. Attempts to establish corresponding factorization theorems fail because of interactions between spectator partons of the colliding hadrons. The contribution of these interactions to the cross section does not decrease with the hard scale. Since they are not associated with the hard-scattering subprocess (see Fig. 13), we no longer have factorization into a parton-level cross section and the parton densities of one of the colliding hadrons. These interactions are generally soft, and we have at present to rely on phenomenological models to quantify their effects [22].

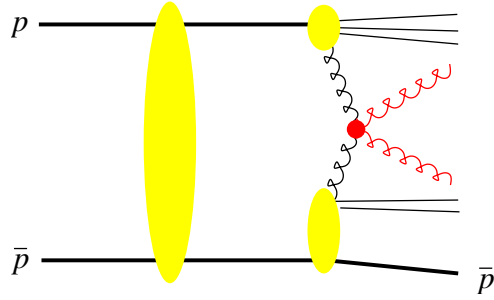


**Fig. 13:** Example graph for diffractive dijet production with a leading antiproton in a  $p\bar{p}$  collision. The interaction indicated by the large vertical blob breaks hard diffractive factorization. It reduces the diffractive cross section, as explained in the text.

The yield of diffractive events in hadron-hadron collisions is lowered precisely because of these soft interactions between spectator partons (often referred to as “reinteractions” or “multiple scatterings”). They can produce additional final-state particles which fill the would-be rapidity gap (hence the often-used term “rapidity gap survival”). When such additional particles are produced, a very fast proton can no longer appear in the final state because of energy conservation. Diffractive factorization breaking is thus intimately related to multiple scattering in hadron-hadron collisions; understanding and describing this phenomenon is a challenge in the high-energy regime that will be reached at the LHC [23].

In  $pp$  or  $p\bar{p}$  reactions, the collision partners are both composite systems of large transverse size, and it is not too surprising that multiple interactions between their constituents can be substantial. In contrast, the virtual photon in  $\gamma^*p$  collisions has small transverse size, which disfavors multiple interactions and enables diffractive factorization to hold. According to our discussion in Sect. 1.2, we may expect that for decreasing virtuality  $Q^2$  the photon behaves more and more like a hadron, and diffractive factorization may again be broken. This aspect of diffractive processes in photoproduction at HERA was intensively discussed during the workshop, and findings are reported in [18].

## 2.5 Space-time structure: the Pomeron is not a particle

It is tempting to interpret diffractive  $\gamma^*p$  processes as the scattering of a virtual photon on a Pomeron which has been radiated off the initial proton. Diffractive DIS would then probe the distribution of partons in a “Pomeron target”. This is indeed the picture proposed by Ingelman and Schlein long ago [24].

This picture is however not supported by an analysis in QCD (see e.g. [25]). There, high-energy scattering is dominated by the exchange of two gluons, whose interaction is (in an appropriate gauge) described by ladder diagrams, as shown in Fig. 14. By analyzing these diagrams in time-ordered perturbation theory, one can obtain the dominant space-time ordering in the high-energy limit. The result depends on the reference frame, as illustrated in the figure. In the Breit frame, which is natural for a parton-model interpretation, the photon does *not* scatter off a parton in a pre-existing two-gluon system; in fact some of the interactions in the gluon ladder building up the Pomeron exchange take place long after the virtual photon has been absorbed. The picture in the Breit frame is however compatible with the interpretation of diffractive parton densities given in Sect. 2.2, namely the probability to find a parton under the condition that subsequent interactions will produce a fast proton in the final state.

We note that the Ingelman-Schlein picture suggests that the diffractive structure function takes a factorized form  $F_2^{D(4)} = f_{\mathbb{P}}(x_{\mathbb{P}}, t) F_2^{\mathbb{P}}(\beta, Q^2)$ , where  $f_{\mathbb{P}}$  is the “Pomeron flux” describing the emission of the Pomeron from the proton and its subsequent propagation, and where  $F_2^{\mathbb{P}}$  is the “structure function of the Pomeron”. Phenomenologically, such a factorizing ansatz works not too badly and is often used, but recent high-precision data have shown its breakdown at small  $x_{\mathbb{P}}$  [15].

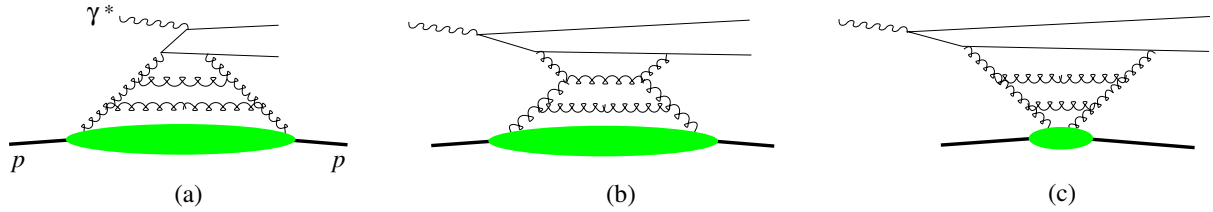


**Fig. 14:** Dominant time ordering for diffractive dissociation of a virtual photon in (a) the Breit frame, (b) the photon-proton center-of-mass, (c) the proton rest frame. The physical picture in (a) corresponds to the parton-model description of diffraction, and the one in (b) and (c) to the picture of the photon splitting into a quark-antiquark dipole which subsequently interacts with the proton.

### 3 Exclusive diffractive processes

Let us now discuss diffractive processes where a real or virtual photon dissociates into a single particle. Since diffraction involves the exchange of vacuum quantum numbers, this particle can in particular be a vector meson (which has the same  $J^{PC}$  quantum numbers as the photon) – in this case the process is sometimes referred to as “elastic” vector meson production. Another important case is deeply virtual Compton scattering (DVCS),  $\gamma^*p \rightarrow \gamma p$ .<sup>3</sup> A striking feature of the data taken at HERA (Figs. 15 and 16) is that the energy dependence of these processes becomes steep in the presence of a hard scale, which can be either the photon virtuality  $Q^2$  or the mass of the meson in the case of  $J/\Psi$  or  $\Upsilon$  production. This is similar to the energy dependence of the  $\gamma^*p$  total cross section (related by the optical theorem to forward Compton scattering,  $\gamma^*p \rightarrow \gamma^*p$ ), which changes from flat to steep when going from real photons to  $Q^2$  of a few  $\text{GeV}^2$ .

To understand this similarity, let us recall that in perturbative QCD diffraction proceeds by two-gluon exchange. The transition from a virtual photon to a real photon or to a quark-antiquark pair subsequently hadronizing into a meson is a short-distance process involving these gluons, provided that either  $Q^2$  or the quark mass is large. In fact, in an approximation discussed below, the cross sections for DVCS and vector meson production are proportional to the square of the gluon distribution in the proton, evaluated at a scale of order  $Q^2 + M_V^2$  and at a momentum fraction  $x_P = (Q^2 + M_V^2)/(W^2 + Q^2)$ , where the vector meson mass  $M_V$  now takes the role of  $M_X$  in inclusive diffraction [28]. In analogy to the case of the total  $\gamma^*p$  cross section, the energy dependence of the cross sections shown in Figs. 15 and 16 thus reflects the  $x$  and scale dependence of the gluon density in the proton, which grows with decreasing  $x$  with a slope becoming steeper as the scale increases.

There is however an important difference in how the gluon distribution enters the descriptions of inclusive DIS and of exclusive diffractive processes. The inclusive DIS cross section is related via the optical theorem to the imaginary part of the forward virtual Compton amplitude, so that the graphs in Fig. 17 represent the *cross section* of the inclusive process. Hence, the gluon distribution in Fig. 17a gives the *probability* to find *one* gluon in the proton (with any number of unobserved spectator partons going into the final state). In contrast, the corresponding graphs for DVCS and exclusive meson production in Fig. 18 represent the *amplitudes* of exclusive processes, which are proportional to the *probability amplitude* for first extracting a gluon from the initial proton and then returning it to form the proton in the final state. In the approximation discussed below, this probability amplitude is given by the gluon distribution. The cross sections of DVCS and exclusive meson production are then proportional to the *square* of the gluon distribution.

A detailed theoretical analysis of DVCS and exclusive meson production at large  $Q^2$  shows that short-distance factorization holds, in analogy to the case of inclusive DIS. QCD factorization theorems [29] state that in the limit of large  $Q^2$  (at fixed Bjorken variable  $x_B$  and fixed  $t$ ) the Compton

<sup>3</sup>We do not discuss processes with diffractive dissociation of the proton in this paper, but wish to mention interesting studies of vector meson or real photon production at large  $|t|$ , where the proton predominantly dissociates, see e.g. [26].

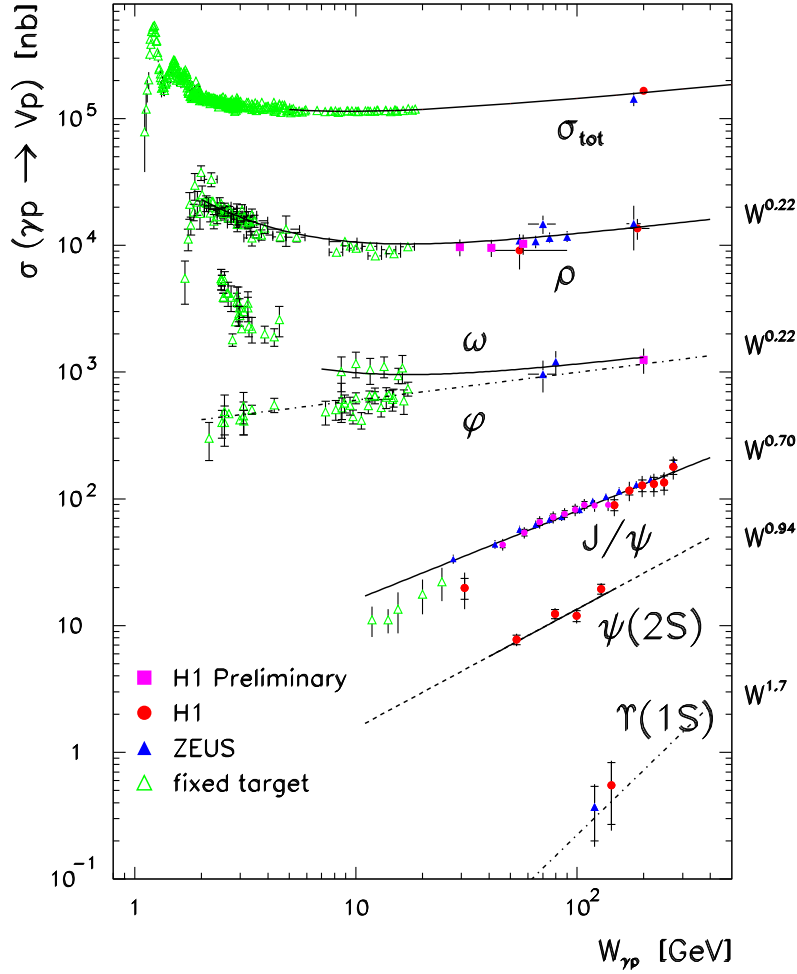


**Fig. 15:** Compilation of results on the cross section for vector meson photoproduction,  $\gamma p \rightarrow Vp$ , with  $V = \rho, \omega, \phi, J/\Psi, \psi', \Upsilon$ , as a function  $W$ . The total  $\gamma p$  cross section  $\sigma_{\text{tot}}$  is also shown.

amplitude factorizes into a hard-scattering subprocess and a hadronic matrix element describing the emission and reabsorption of a parton by the proton target (see Fig. 18a). As shown in Fig. 18b, the analogous result for exclusive meson production involves in addition the quark-antiquark distribution amplitude of the meson (often termed the meson wave function) and thus a further piece of non-perturbative input.

The hadronic matrix elements appearing in the factorization formulae for exclusive processes would be the usual PDFs if the proton had the same momentum in the initial and final state. Since this is not the case, they are more general functions taking into account the momentum difference between the initial and final state proton (or, equivalently, between the emitted and reabsorbed parton). These “generalized parton distributions” (GPDs) depend on two independent longitudinal momentum fractions instead of a single one (compare Figs. 17a and 18a), on the transverse momentum transferred to the proton (whose square is  $-t$  to a good approximation at high energy), and on the scale at which the partons are probed. The scale dependence of the GPDs is governed by a generalization of the DGLAP equations. The dependence on the difference of the longitudinal momenta (often called “skewness”) contains information on correlations between parton momenta in the proton wave function. It can be neglected in the approximation of leading  $\log x$  (then the GPDs at  $t = 0$  reduce to the usual PDFs as anticipated above), but it is numerically important in typical HERA kinematics. The dependence on  $t$  allows for a very intuitive interpretation if a Fourier transformation is performed with respect to the transverse momentum transfer. We then obtain distributions depending on the impact parameter of the

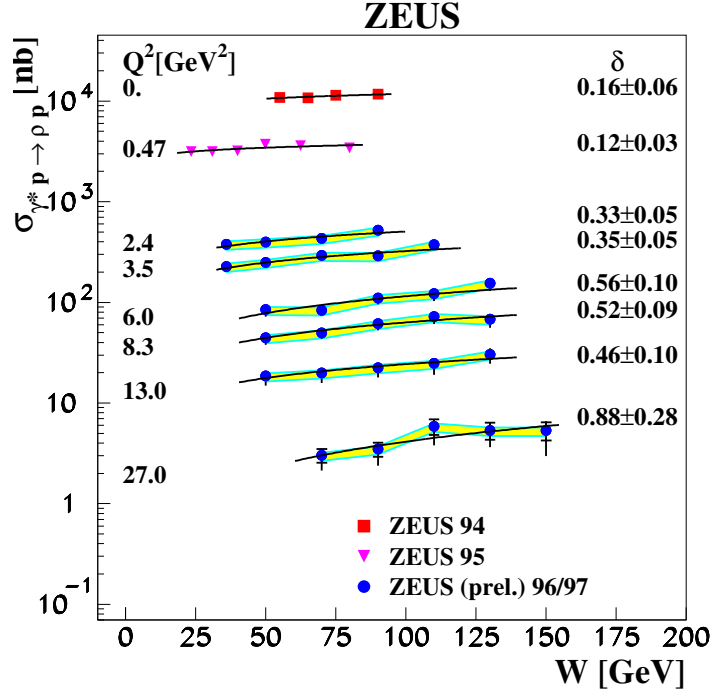


**Fig. 16:** Cross section for exclusive  $\rho$  production as a function of  $W$  (from [27]). The lines represent the result of fits to the data with the form  $\sigma(\gamma^*p \rightarrow \rho p) \propto W^\delta$ , yielding the exponents given in the figure.

partons, which describe the two-dimensional distribution of the struck parton in the transverse plane, and on its longitudinal momentum fraction in the proton. The  $t$  dependence of exclusive diffractive processes thus provides unique information beyond the longitudinal momentum spectra encoded in the usual parton densities. The study of the generalized parton distributions is a prime reason to measure DVCS and exclusive meson production in  $ep$  scattering. Detailed discussions and references can be found in the recent reviews [30,31].

An observable illustrating the short-distance factorization in meson production at high  $Q^2$  is the ratio of the  $\phi$  and  $\rho$  production cross sections, shown in Fig. 19. At large  $Q^2$  the process is described in terms of a light quark coupling to the photon and of the generalized gluon distribution. Using approximate flavor SU(3) symmetry between the  $\rho$  and  $\phi$  wave functions, the only difference between the two channels is then due to different quark charge and isospin factors, which result in a cross section ratio of  $2/9$ .

### 3.1 High-energy factorization and the dipole picture

So far we have discussed the description of hard exclusive diffraction within short-distance, or collinear factorization. A different type of factorization is high-energy, or  $k_t$  factorization, which is based on the BFKL formalism. Here the usual or generalized gluon distribution appearing in the factorization formulae depends explicitly on the transverse momentum  $k_t$  of the emitted gluon. In collinear factorization, this  $k_t$  is integrated over in the parton distributions and set to zero when calculating the hard-scattering process (the partons are thus approximated as “collinear” with their parent hadron). Likewise, the meson wave functions appearing in  $k_t$  factorization explicitly depend on the relative transverse momentum between the quark and antiquark in the meson, whereas this is integrated over in the quark-antiquark distribution amplitudes (cf. Sect. 3) of the collinear factorization formalism. Only gluon distributions appear in  $k_t$  factorization, whereas collinear factorization formulae involve both quark and gluon distributions (see e.g. Sects. 8.1 and 8.2 in [30] for a discussion of this difference). We note that other

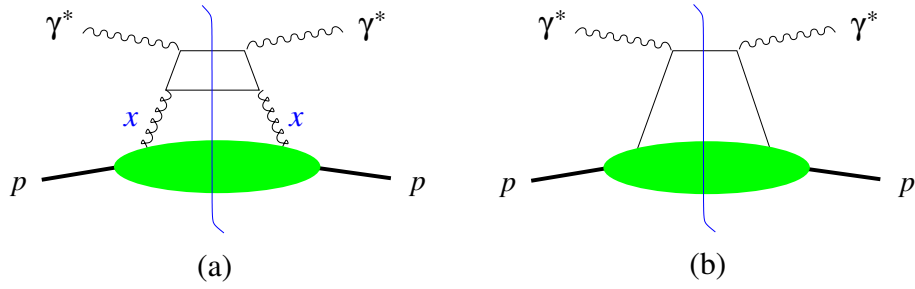


**Fig. 17:** Factorization of forward Compton scattering, which is related to the total inclusive structure function via the optical theorem,  $\text{Im } \mathcal{A}(\gamma^* p \rightarrow \gamma^* p) = \frac{1}{2} \sum_X |\mathcal{A}(\gamma^* p \rightarrow X)|^2 \propto \sigma(\gamma^* p \rightarrow X)$ . The final state of the inclusive process is obtained by cutting the diagrams along the vertical line. The blobs represent the gluon or quark distribution in the proton. Graph (b) is absent in the  $k_t$  factorization formalism (see Sect. 3.1): its role is taken by graph (a) in the “aligned jet configuration”, where the quark line joining the two photons carries almost the entire photon momentum.

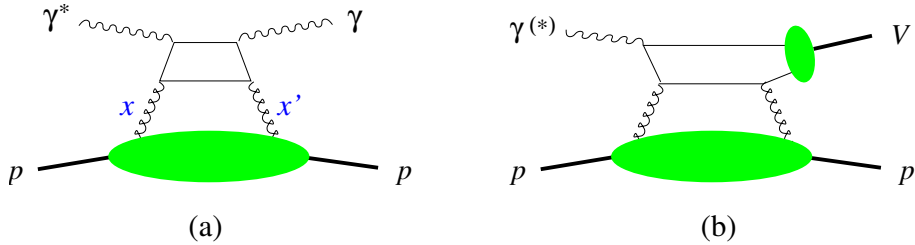


**Fig. 18:** (a) Factorization of deeply virtual Compton scattering,  $\gamma^* p \rightarrow \gamma p$ , which can be measured in the exclusive process  $ep \rightarrow ep\gamma$ . The blob represents the generalized gluon distribution, with  $x$  and  $x'$  denoting the momentum fractions of the gluons. (b) Factorization of exclusive meson production. The small blob represents the vector meson wave function. In the collinear factorization formalism, there are further graphs (not shown) involving quark instead of gluon exchange.

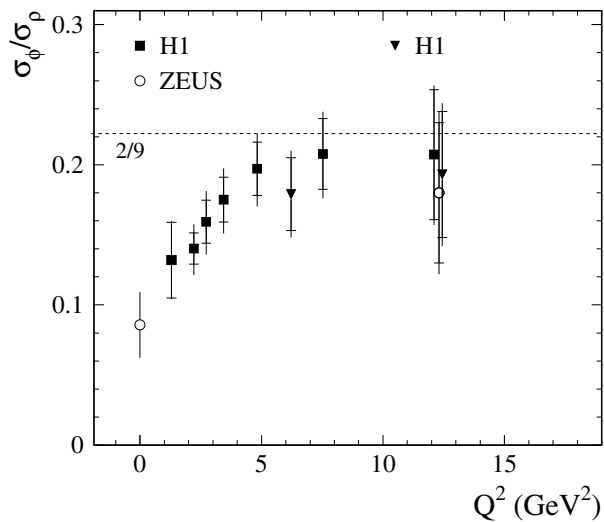


**Fig. 19:** The ratio of cross sections for  $\gamma^* p \rightarrow \phi p$  and  $\gamma^* p \rightarrow \rho p$  as a function of the photon virtuality (from [32]).

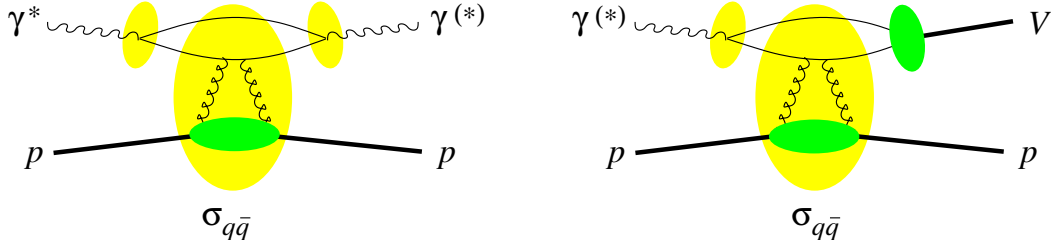


**Fig. 20:** The dipole representation of the amplitudes for Compton scattering (a) and for meson production (b), corresponding to the graphs in Figs. 17a and 18.

factorization schemes have been developed, which combine features of the collinear and  $k_t$  factorization formalisms.

The two different types of factorization implement different ways of separating different parts of the dynamics in a scattering process. The building blocks in a short-distance factorization formula correspond to either small or large particle virtuality (or equivalently to small or large transverse momentum), whereas the separation criterion in high-energy factorization is the particle rapidity. Collinear and  $k_t$  factorization are based on taking different limits: in the former case the limit of large  $Q^2$  at fixed  $x_B$  and in the latter case the limit of small  $x_B$  at fixed  $Q^2$  (which must however be large enough to justify the use of QCD perturbation theory). In the common limit of large  $Q^2$  and small  $x_B$  the two schemes give coinciding results. Instead of large  $Q^2$  one can also take a large quark mass in the limits just discussed.

A far-reaching representation of high-energy dynamics can be obtained by casting the results of  $k_t$  factorization into a particular form. The different building blocks in the graphs for Compton scattering and meson production in Figs. 17a and 18 can be rearranged as shown in Fig. 20. The result admits a very intuitive interpretation in a reference frame where the photon carries large momentum (this may be the proton rest frame but also a frame where the proton moves fast, see Fig. 14): the initial photon splits into a quark-antiquark pair, which scatters on the proton and finally forms a photon or meson again. This is the picture we have already appealed to in Sect. 1.2.

In addition, one can perform a Fourier transformation and trade the relative transverse momentum between quark and antiquark for their transverse distance  $r$ , which is conserved in the scattering on the target. The quark-antiquark pair acts as a color dipole, and its scattering on the proton is described by a “dipole cross section”  $\sigma_{q\bar{q}}$  depending on  $r$  and on  $x_P$  (or on  $x_B$  in the case of inclusive DIS). The wave functions of the photon and the meson depend on  $r$  after Fourier transformation, and at small  $r$  the photon wave function is perturbatively calculable. Typical values of  $r$  in a scattering process are determined by the inverse of the hard momentum scale, i.e.  $r \sim (Q^2 + M_V^2)^{-1/2}$ . An important result of high-energy factorization is the relation

$$\sigma_{q\bar{q}}(r, x) \propto r^2 x g(x) \quad (7)$$

at small  $r$ , where we have replaced the generalized gluon distribution by the usual one in the spirit of the leading  $\log x$  approximation. A more precise version of the relation (7) involves the  $k_t$  dependent gluon distribution. The dipole cross section vanishes at  $r = 0$  in accordance with the phenomenon of “color transparency”: a hadron becomes more and more transparent for a color dipole of decreasing size.

The scope of the dipole picture is wider than we have presented so far. It is tempting to apply it outside the region where it can be derived in perturbation theory, by modeling the dipole cross section and the photon wave function at large distance  $r$ . This has been very fruitful in phenomenology, as we will see in the next section.

The dipole picture is well suited to understand the  $t$  dependence of exclusive processes, parameterized as  $d\sigma/dt \propto \exp(-b|t|)$  at small  $t$ . Figure 21 shows that  $b$  decreases with increasing scale  $Q^2 + M_V^2$

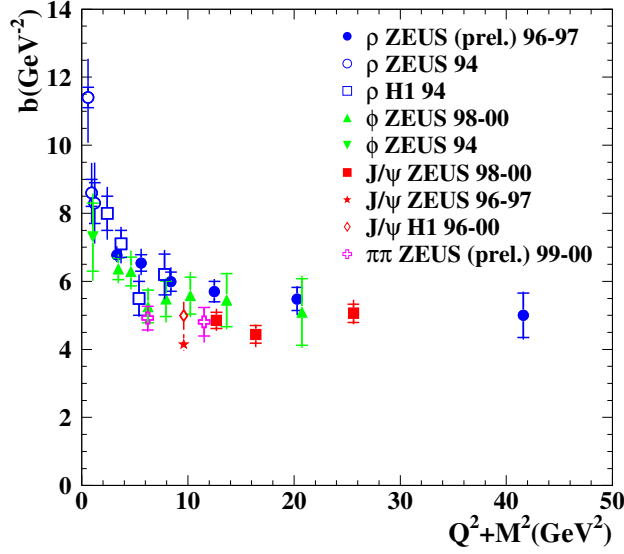


**Fig. 21:** The logarithmic slope of the  $t$  dependence at  $t = 0$  for different meson production channels, as well as for non-resonant dipion production.

and at high scales becomes independent of the produced meson. A Fourier transform from momentum to impact parameter space readily shows that  $b$  is related to the typical transverse distance between the colliding objects, as anticipated by the analogy with optical diffraction in Sect. 1.1. At high scale, the  $q\bar{q}$  dipole is almost pointlike, and the  $t$  dependence of the cross section is controlled by the  $t$  dependence of the generalized gluon distribution, or in physical terms, by the transverse extension of the proton. As the scale decreases, the dipole acquires a size of its own, and in the case of  $\rho$  or  $\phi$  photoproduction, the values of  $b$  reflect the fact that the two colliding objects are of typical hadronic dimensions; similar values would be obtained in elastic meson-proton scattering.

### 3.2 Exclusive diffraction in hadron-hadron collisions

The concepts we have introduced to describe exclusive diffraction can be taken over to  $pp$  or  $p\bar{p}$  scattering, although further complications appear in these processes. A most notable reaction is exclusive production of a Higgs boson,  $pp \rightarrow pHp$ , sketched in Fig. 22. The generalized gluon distribution is a central input in this description. The physics interest, theory description, and prospects to measure this process at the LHC have been discussed in detail at this workshop [33, 34]. A major challenge in the description of this process is to account for secondary interactions between spectator partons of the two projectiles, which can produce extra particles in the final state and hence destroy the rapidity gaps between the Higgs and final-state protons – the very same mechanism we discussed in Sect. 2.4.

## 4 Parton saturation

We have seen that diffraction involves scattering on small- $x$  gluons in the proton. Consider the density in the transverse plane of gluons with longitudinal momentum fraction  $x$  that are resolved in a process with hard scale  $Q^2$ . One can think of  $1/Q$  as the “transverse size” of these gluons as seen by the probe. The number density of gluons at given  $x$  increases with increasing  $Q^2$ , as described by DGLAP evolution (see Fig. 23). According to the BFKL evolution equation it also increases at given  $Q^2$  when  $x$  becomes smaller, so that the gluons become more and more densely packed. At some point, they will start to overlap and thus reinteract and screen each other. One then enters a regime where the density of partons

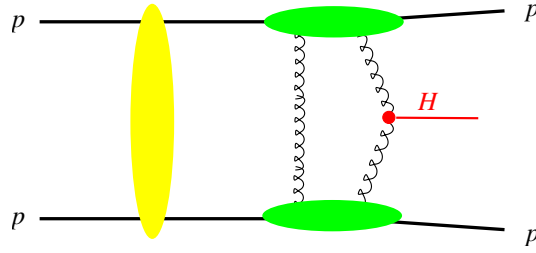


**Fig. 22:** Graph for the exclusive production of a Higgs boson in  $pp$  scattering. The horizontal blobs indicate generalized gluon distributions, and the vertical blob represents secondary interactions between the projectiles (cf. Fig. 13).

saturates and where the linear DGLAP and BFKL evolution equations cease to be valid. If  $Q^2$  is large enough to have a small coupling  $\alpha_s$ , we have a theory of this non-linear regime called “color glass condensate”, see e.g. [35]. To quantify the onset of non-linear effects, one introduces a saturation scale  $Q_s^2$  depending on  $x$ , such that for  $Q^2 < Q_s^2(x)$  these effects become important. For smaller values of  $x$ , the parton density in the target proton is higher, and saturation sets in at larger values of  $Q^2$  as illustrated in Fig. 23.

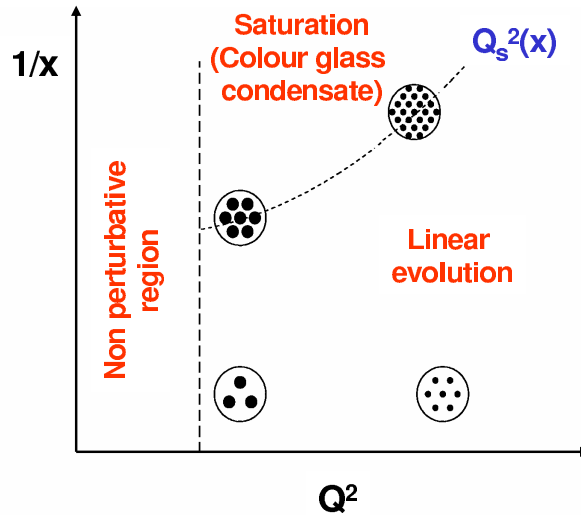


**Fig. 23:** Schematic view of the density of gluons in the transverse plane, as a function of the momentum fraction  $x$  and the resolution scale  $Q^2$ . Above the line given by  $Q_s^2(x)$ , saturation effects set in.

The dipole picture we introduced in Sect. 3.1 is well suited for the theoretical description of saturation effects. When such effects are important, the relation (7) between dipole cross section and gluon distribution ceases to be valid; in fact the gluon distribution itself is then no longer an adequate quantity to describe the dynamics of a scattering process. In a certain approximation, the evolution of the dipole cross section with  $x$  is described by the Balitsky-Kovchegov equation [36], which supplements the BFKL equation with a non-linear term taming the growth of the dipole cross section with decreasing  $x$ .

Essential features of the saturation phenomenon are captured in a phenomenological model for the dipole cross section, originally proposed by Golec-Biernat and Wüsthoff, see [37, 38]. Figure 24 shows  $\sigma_{q\bar{q}}$  as a function of  $r$  at given  $x$  in this model. The dipole size  $r$  now plays the role of  $1/Q$  in our discussion above. At small  $r$  the cross section rises following the relation  $\sigma_{q\bar{q}}(r, x) \propto r^2 x g(x)$ . At some value  $R_s(x)$  of  $r$ , the dipole cross section is so large that this relation ceases to be valid, and  $\sigma_{q\bar{q}}$

starts to deviate from the quadratic behavior in  $r$ . As  $r$  continues to increase,  $\sigma_{q\bar{q}}$  eventually saturates at a value typical of a meson-proton cross section. In terms of the saturation scale introduced above,  $R_s(x) = 1/Q_s(x)$ . For smaller values of  $x$ , the initial growth of  $\sigma_{q\bar{q}}$  with  $r$  is stronger because the gluon distribution is larger. The target is thus more opaque and as a consequence saturation sets in at lower  $r$ .

A striking feature found both in this phenomenological model [39] and in the solutions of the Balitsky-Kovchegov equation (see e.g. [40]) is that the total  $\gamma^*p$  cross section only depends on  $Q^2$  and  $x_B$  through a single variable  $\tau = Q^2/Q_s^2(x_B)$ . This property, referred to as geometric scaling, is well satisfied by the data at small  $x_B$  (see Fig. 25) and is an important piece of evidence that saturation effects are visible in these data. Phenomenological estimates find  $Q_s^2$  of the order 1 GeV<sup>2</sup> for  $x_B$  around  $10^{-3}$  to  $10^{-4}$ .

The dipole formulation is suitable to describe not only exclusive processes and inclusive DIS, but also inclusive diffraction  $\gamma^*p \rightarrow Xp$ . For a diffractive final state  $X = q\bar{q}$  at parton level, the theory description is very similar to the one for deeply virtual Compton scattering, with the wave function for the final state photon replaced by plane waves for the produced  $q\bar{q}$  pair. The inclusion of the case  $X = q\bar{q}g$  requires further approximations [37] but is phenomenologically indispensable for moderate to small  $\beta$ . Experimentally, one observes a very similar energy dependence of the inclusive diffractive and the total cross section in  $\gamma^*p$  collisions at given  $Q^2$  (see Fig. 26). The saturation mechanism implemented in the Golec-Biernat Wüsthoff model provides a simple explanation of this finding. To explain this aspect of the data is non-trivial. For instance, in the description based on collinear factorization, the energy dependence of the inclusive and diffractive cross sections is controlled by the  $x$  dependence of the ordinary and the diffractive parton densities. This  $x$  dependence is not predicted by the theory.

The description of saturation effects in  $pp$ ,  $pA$  and  $AA$  collisions requires the full theory of the color glass condensate, which contains concepts going beyond the dipole formulation discussed here and is e.g. presented in [35]. We remark however that estimates of the saturation scale  $Q_s^2(x)$  from HERA data can be used to describe features of the recent data from RHIC [41].

## 5 A short summary

Many aspects of diffraction in  $ep$  collisions can be successfully described in QCD if a hard scale is present. A key to this success are factorization theorems, which render parts of the dynamics accessible to calculation in perturbation theory. The remaining non-perturbative quantities, namely diffractive PDFs and generalized parton distributions, can be extracted from measurements and contain specific information about small- $x$  partons in the proton that can only be obtained in diffractive processes. To describe hard diffractive hadron-hadron collisions is more challenging since factorization is broken by rescattering between spectator partons. These rescattering effects are of interest in their own right because of their intimate relation with multiple scattering effects, which at LHC energies are expected to be crucial for understanding the structure of events in hard collisions. A combination of data on inclusive and diffractive  $ep$  scattering hints at the onset of parton saturation at HERA, and the phenomenology developed there is a helpful step towards understanding high-density effects in hadron-hadron collisions.

## Acknowledgements

It is a pleasure to thank our co-convenors and all participants for the fruitful atmosphere in the working group on diffraction, and A. De Roeck and H. Jung for their efforts in organizing this workshop. We are indebted to A. Proskuryakov for Figs. 5 and 12, to P. Fleischmann for Fig. 15, and to A. Bonato, K. Borras, A. Bruni, J. Forshaw, M. Grothe, H. Jung, L. Motyka, M. Ruspa and M. Wing for valuable comments on the manuscript.

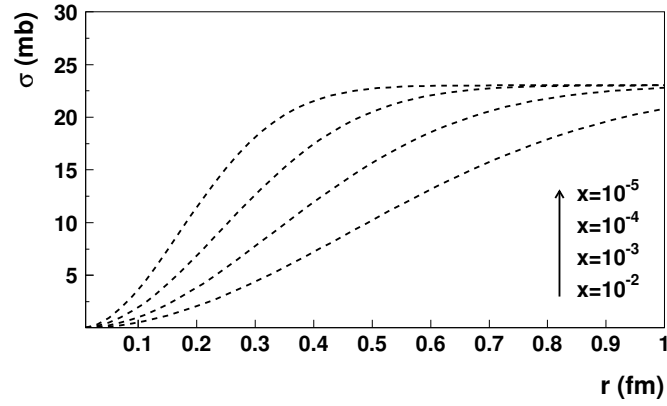


**Fig. 24:** The dipole cross section  $\sigma_{q\bar{q}}$  in the Golec-Biernat Wüsthoff model as a function of dipole size  $r$  for different  $x$  (from [38]).

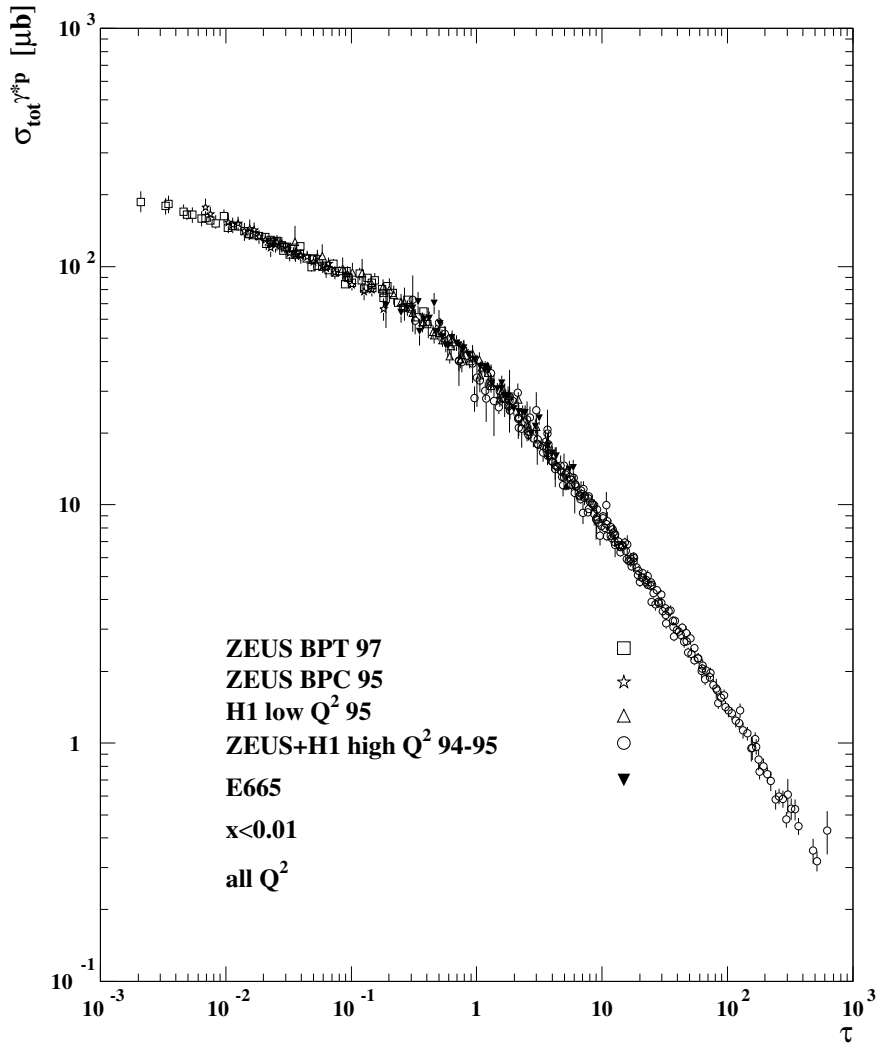


**Fig. 25:** Geometric scaling of the  $\gamma^*p$  cross section in a single variable  $\tau = Q^2/Q_s^2(x_B)$ , as determined in [39]. The  $Q^2$  of these data ranges from 0.045 to 450 GeV<sup>2</sup>.

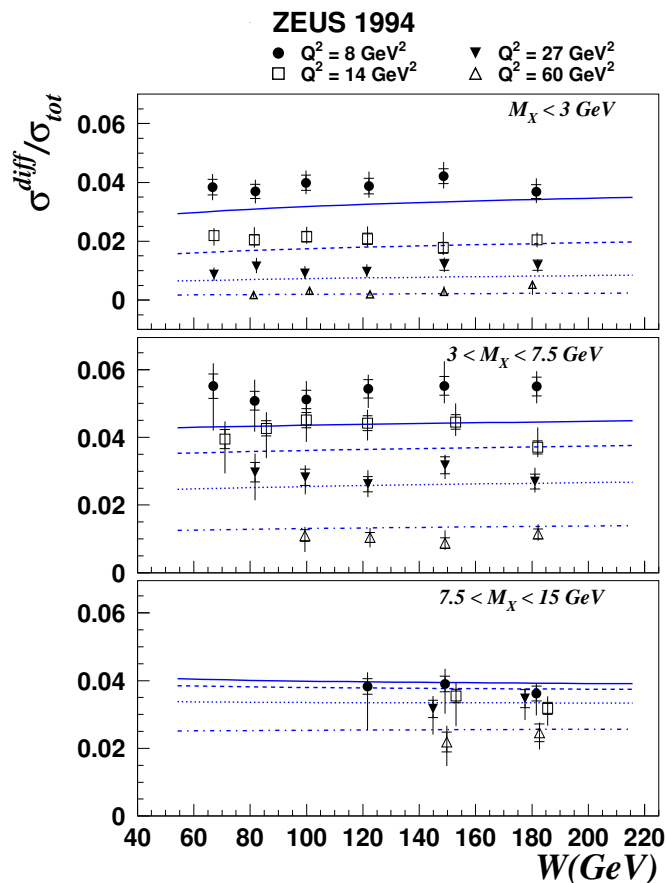


**Fig. 26:** Data on the ratio of diffractive and total  $\gamma^*p$  cross sections compared with the result of the Golec-Biernat Wüsthoff model (from [37]).

## References

- [1] P. D. B. Collins, *An Introduction to Regge Theory and High-Energy Physics*, Cambridge University Press, Cambridge, 1977.
- [2] E. A. Kuraev, L. N. Lipatov and V. S. Fadin, *Sov. Phys. JETP* **44** (1976) 443; *ibid.* **45** (1977) 199; I. I. Balitsky and L. N. Lipatov, *Sov. J. Nucl. Phys.* **28** (1978) 822.
- [3] J. R. Forshaw and D. A. Ross, *Quantum chromodynamics and the pomeron*, Cambridge Lect. Notes Phys. **9** (1997) 1; A. Hebecker, *Phys. Rept.* **331** (2000) 1 [hep-ph/9905226]; M. Wüsthoff and A. D. Martin, *J. Phys. G* **25** (1999) R309 [hep-ph/9909362]; V. Barone and E. Predazzi, *High-energy particle diffraction*, Springer, 2002; I. P. Ivanov, N. N. Nikolaev and A. A. Savin, hep-ph/0501034.
- [4] K. Goulianos, *Phys. Rept.* **101** (1983) 169.
- [5] G. Bruni *et al.*, these proceedings.
- [6] S. Chekanov *et al.* [ZEUS Collaboration], *Eur. Phys. J. C* **38** (2004) 43 [hep-ex/0408009].
- [7] H1 Collaboration, Paper 89 submitted to the International Europhysics Conference on High Energy Physics (EPS 2003), July 2003, Aachen, Germany, available from <http://www-h1.desy.de>
- [8] ZEUS Collaboration, Paper 1048 submitted to the 30th International Conference on High Energy Physics (ICHEP 2000), July–August 2000, Osaka, Japan, available from <http://www-zeus.desy.de>
- [9] S. Chekanov *et al.* [ZEUS Collaboration], *Eur. Phys. J. C* **21** (2001) 443 [hep-ex/0105090].
- [10] L. Trentadue and G. Veneziano, *Phys. Lett. B* **323** (1994) 201.

- [11] A. Berera and D. E. Soper, Phys. Rev. D **53** (1996) 6162 [hep-ph/9509239].
- [12] J. C. Collins, Phys. Rev. D **57** (1998) 3051, Erratum ibid. D **61** (2000) 019902 [hep-ph/9709499].
- [13] P. Newman and F.-P. Schilling, these proceedings.
- [14] M. Groys, A. Levy and A. Proskuryakov, these proceedings.
- [15] S. Chekanov *et al.* [ZEUS Collaboration], Nucl. Phys. B **713** (2005) 3 [hep-ex/0501060].
- [16] A. D. Martin, M. G. Ryskin and G. Watt, Eur. Phys. J. C **37** (2004) 285 [hep-ph/0406224];  
A. D. Martin, M. G. Ryskin and G. Watt, these proceedings.
- [17] H1 Collaboration, Paper 6-0177 submitted to the 32nd International Conference on High Energy Physics (ICHEP 2004), August 2004, Beijing, China, available from <http://www-h1.desy.de>
- [18] A. Bruni *et al.*, these proceedings [hep-ph/0509202].
- [19] T. Affolder *et al.* [CDF Collaboration], Phys. Rev. Lett. **84** (2000) 5043.
- [20] L. Alvero *et al.*, Phys. Rev. D **59** (1999) 074022 [hep-ph/9805268].
- [21] A. Proskuryakov, Y. Yamazaki and M. Arneodo, presented at the HERA-LHC Workshop, 11–13 October 2004, CERN, <http://agenda.cern.ch/fullAgenda.php?ida=a044163>
- [22] E. Gotsman *et al.*, these proceedings.
- [23] J. Bartels, M. Salvadore and G. P. Vacca, Eur. Phys. J. C **42** (2005) 53 [hep-ph/0503049];  
J. Bartels, these proceedings,  
C. Buttar *et al.*, these proceedings.
- [24] G. Ingelman and P. E. Schlein, Phys. Lett. B **152** (1985) 256.
- [25] J. Bartels and M. G. Ryskin, Z. Phys. C **76** (1997) 241 [hep-ph/9612226].
- [26] R. Enberg *et al.*, hep-ph/0407328;  
S. Chekanov *et al.* [ZEUS Collaboration], Eur. Phys. J. C **26** (2003) 389 [hep-ex/0205081];  
A. Aktas *et al.* [H1 Collaboration], Phys. Lett. B **568** (2003) 205 [hep-ex/0306013].
- [27] ZEUS Collaboration, Paper 594 submitted to the International Europhysics Conference on High Energy Physics (EPS 2001), July 2001, Budapest, Hungary, available from <http://www-zeus.desy.de>
- [28] M. G. Ryskin, Z. Phys. C **57** (1993) 89.
- [29] J. C. Collins, L. Frankfurt and M. Strikman, Phys. Rev. D **56** (1997) 2982 [hep-ph/9611433];  
J. C. Collins and A. Freund, Phys. Rev. D **59** (1999) 074009 [hep-ph/9801262].
- [30] M. Diehl, Phys. Rept. **388**, 41 (2003) [hep-ph/0307382].
- [31] A. V. Belitsky and A. V. Radyushkin, hep-ph/0504030.
- [32] C. Adloff *et al.* [H1 Collaboration], Phys. Lett. B **483** (2000) 360 [hep-ex/0005010].
- [33] Contributions to these proceedings by J. Kalliopuska *et al.*; V. Avati and K. Österberg; M. Arneodo *et al.*; V. Andreev *et al.*
- [34] J. Forshaw, these proceedings [hep-ph/0508274];  
M. Boonekamp *et al.*, these proceedings.
- [35] H. Weigert, hep-ph/0501087;  
R. Venugopalan, these proceedings.
- [36] I. Balitsky, Nucl. Phys. B **463** (1996) 99 [hep-ph/9509348];  
Y. V. Kovchegov, Phys. Rev. D **61** (2000) 074018 [hep-ph/9905214].
- [37] K. Golec-Biernat and M. Wüsthoff, Phys. Rev. D **60** (1999) 114023 [hep-ph/9903358].
- [38] K. Golec-Biernat, Acta Phys. Polon. B **33** (2002) 2771 [hep-ph/0207188].
- [39] A. M. Stasto, K. Golec-Biernat and J. Kwiecinski, Phys. Rev. Lett. **86** (2001) 596 [hep-ph/0007192].
- [40] K. Golec-Biernat, L. Motyka and A. M. Stasto, Phys. Rev. D **65** (2002) 074037 [hep-ph/0110325];  
M. Lublinsky, Eur. Phys. J. C **21** (2001) 513 [hep-ph/0106112];  
S. Munier and R. Peschanski, Phys. Rev. Lett. **91** (2003) 232001 [hep-ph/0309177].
- [41] D. Kharzeev and E. Levin, Phys. Lett. B **523** (2001) 79 [nucl-th/0108006];  
A. Krasnitz, Y. Nara and R. Venugopalan, Nucl. Phys. A **727** (2003) 427 [hep-ph/0305112].